Journal of Harbin Engineering University
ISSN: 1006-7043

Vol 46 No. 1
March 2025

Dynamic Analysis of Axial Piston Pumps under Uncertainty using Karhunen–Loève Decomposition

Van Hai Trinh[a], Duong Vu[1,*], Duy Trung Dao[c]

[a] Institute of Vehicle and Energy Engineering, Le Quy Don Technical University, 236, Hoang Quoc Viet, Hanoi, Vietnam

[b] Duy Tan University, Danang, Vietnam

[c] Institute of Mechanical Engineering, Hanoi, Vietnam

Abstract

Hydraulic systems are commonly employed in industrial systems and machinery due to their advanced characteristics. Among these, axial piston pumps, as the primary component, play a key role in developments and refinements of modern hydraulic systems. In this study, the Karhunen-Loève (KL) expansion is employed to analyse the pump dynamic characteristics (i.e., outlet pressure and flow rate). A dynamic model of the axial piston pump is formulated to investigate the pump dynamic behaviors using the numerical Runge-Kutta (RK) scheme at a reasonable convergence level. Subsequently, surrogate models are reconstructed using a truncated KL expansion to analyse the pump dynamic responses while accounting uncertainties of system parameters in a high-dimensional space. The results demonstrate that, with a convergence level at a relative error of 1×10^{-7}, the forth-order truncated surrogate model shows a strong predictive capability in characterizing the pump dynamic responses having transition regions. Additionally, in terms of uncertainty quantification, pump characteristics appear to follow a normal distribution function regardless of whether the input system parameters are normally or uniformly distributed.

Keywords: Axial piston pump, dynamic response, pump pressure, outlet flow rate, reduced-order model, Karhunen-Loève expansion

1. Introduction

Hydraulic systems are fundamental to the functionality of industrial system and mobile machinery, enabling the execution of high-power and precision-driven operations, including lifting, pressing, and transporting substantial loads. These systems are extensively implemented in sectors such as construction, agriculture, aerospace, and industrial manufacturing, where their advantages —such as exceptional power density, precise modulation of forces and torques, and accurate control of motion and positioning—are critical. The incorporation of hydraulic technology into automated heavy machinery has led to substantial advancements in industrial processes, enhancing operational efficiency and ensuring improved safety standards [1, 2]. Axial piston pumps are essential components of hydraulic systems, converting mechanical energy into fluid flow energy with a wide operating pressure range, depending on actual usage requirements [3, 4]. Constructing a dynamic model for axial piston pumps is essential for evaluating their operational behavior across a range of working conditions. These constructed models enable to characterize the pump performance characteristics, including pressure fluctuations, flow dynamics, and mechanical interactions, which provide a comprehensive assessment of efficiency, performance, and stability. By capturing the complex interplay between hydraulic and mechanical components, this approach facilitates the optimization of pump design and control strategies, ensuring reliable and efficient functionality in real applications [4–9].

Dynamic models of axial piston pumps have been extensively explored [5, 10–12]. W. Latas and J. Stojek [11] developed a 13-DOF dynamic pump model considering the relationship between the wear level of the components and the stiffness and viscous damping parameters of the connections. The phase trajectory calculated at certain observation points provides information for assessing the wear condition of the components. Similarly, effects of the working conditions (i.e., outlet pressure, rotating speed, and displacement angle) and structural parameters (i.e., stiffness and damping coefficients of different contact zones such as piston-cylinder bore, cylinder-valve plate, and slipper-swash plate) on the dynamic responses

(i.e., amplitude-frequency vibration, phase trajectory diagram) are investigated with 8-DOF [5] and 19-DOF [12] dynamic model. To solve dynamic models of pump systems, various methods have been developed depending on the model complexity and research objectives: CFD model [13], numerical integration (i.e., RK scheme [5], Newmark-β method [12]), commercial tool (i.e., Matlab-Simulink [8, 9] AMESim [15]), or hybrid/combined approaches [12, 16]. Thanks to these computational tools and techniques, some dynamic behaviors of axial piston pumps can be assessed, with the flow rate [13, 14] and outlet pressure [15, 17] ripples; as typical examples. Ensuring the reliable operation and extended lifespan of hydraulic piston pumps necessitates effective monitoring strategies to mitigate the risk of unexpected failures during the process of use and operation. Thanks to the mathematical and dynamic models developed above, advanced diagnostic methodologies typically involve the continuous acquisition of real-time data on key operational parameters, including pressure, temperature, flow rate, and leakage [4, 18–20]. These critical indicators facilitate the early identification of wear and potential malfunctions in essential components such as pistons and cylinder block. By integrating sensor technology with intelligent diagnostic software, maintenance teams can proactively identify deviations from normal performance, enabling timely corrective measures. Furthermore, predictive maintenance frameworks leveraging these monitoring techniques enhance system reliability by minimizing unplanned downtime, optimizing operational efficiency, and prolonging the service life of hydraulic pumps [25–27]. It can be stated that the system parameters and the structural characteristics of hydraulic components are often not deterministic in practice. Therefore, the problem of studying the system dynamics must be addressed [28–32]. Within mismatched uncertainties, the challenges in controlling variable-speed pump-controlled hydraulic systems were addressed [28]. The study examines the uncertainties related to measuring pump efficiency, with the goal of establishing appropriate confidence intervals and precisely evaluating the pump's performance and dynamic behavior [29]. The uncertainty quantification frameworks are also extended to research for similar elements such as centrifugal pumps [30, 31] and hydraulic actuators [32]. In this work, we develop a computational model to analyse the working characteristics of the axial piston pump using a reduced-order surrogate based on KL expansion. To achieve this objective, the remainder of the paper is structured as follows. In Section 3.1, we introduce the dynamic model of the pump considering the piston pressure and the pump outlet pressure as working parameters. In Section 3.2, the RK scheme and KL expansion, as applied to the pump dynamics problem, are presented. The outlet pressure and flow characteristics of the pump are discussed in Section 4, following an assessment of the convergence properties of the numerical 2 calculations. To sum up, some concluding remarks are provided in Section 5.

2. Dynamic model of axial piston pump

This section will present the typical structure and operation of an axial piston pump. After that, a system of differential equations will be formulated for describing the dynamic characteristics of the pump system such as outlet pressure and flow rate responses.

2.1. Description of axial piston pump structure

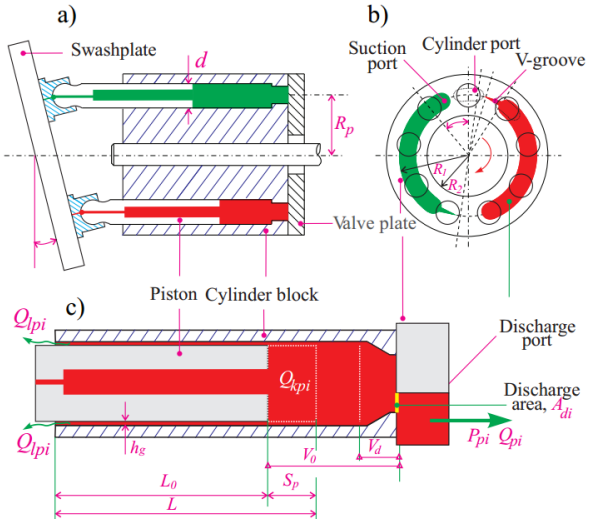

Figure 1: Structure and geometrical/operational parameters of an axial piston pump

The functional principle and geometrical/ operational parameters of an axial piston pump are depicted in Fig. 1. This pump system has some primary components like swashplate, pistons, cylinder block, and valve plate (see Fig. 1a). In the operation process, the drive motor or engine supplies rotational motion to the pump shaft, which then rotates the cylinder block, leading pump pistons in motion. The swashplate, inclined at a specific angle (i.e., β) relative to the cylinder block, plays a critical role in creating alternating suction and discharge strokes for each piston as it rotates. This inclination causes each piston to follow a reciprocating motion, drawing in hydraulic fluid during the suction

phase and expelling it during the discharge phase. The valve plate (positioned at the piston base, Fig. 1b) directs hydraulic oil from the suction port into the piston chambers and facilitates the exit of pressurized fluid through the discharge port, enabling controlled fluid flow through the pump system. Details of the symbols shown in Fig. 1 and their descriptions will be covered in Section 3.1.2. It should be noted that in modern pumping systems, the above pump structure will be integrated 3 with control valve system control flow, working pressure as well as achieve other advanced functions of the system in terms of drive and control quality, as well as self-protection and self-diagnosis features.

One of the problems that needs to be addressed in the design and operation of axial piston pump systems is studying the relationship between dynamic characteristics (i.e., pressure and flow rate) between the single piston chambers and the pump discharge chamber, taking into account the influence of structural/operational parameters and hydraulic oil properties.

2.2. Dynamic modeling

Mathematical formulas representing the dynamic model of the pump system can be stated through the following equations for the piston instantaneous pressure and the pump output pressure. For the pump piston system, their instantaneous pressure can be formulated by [21]:

$$\dot{P}_{pi}=\frac{B}{V_0-A_pS_{pi}}\left(Q_{kpi}-Q_{pi}-Q_{lpi}\right), \tag{2.1}$$

where B is the bulk modulus of hydraulic oil, V_0 denotes the initial volume of the piston, and A_p denotes the piston area. The stroke S_{pi} the i-th piston is given as:

$$S_{pi}=R_p\tan\beta(1-\cos\Omega_i), \tag{2.2}$$

with R_p represents the piston pitch radius, $\Omega_i=\omega t-(i-1)\alpha$ is the angular position of the i–th piston, α is phase delay, β is the swash-plate angle, and ω refers to the rotational speed of the pump shaft.

The right-side expression of Eq. (2.1) includes the kinematic flow Q_{kpi}, the flow discharge Q_{pi}, and the internal leakage Q_{lpi} associated with the i–th piston (see Fig. 1c), which are defined by the following equations:

$$Q_{kpi}=\omega\frac{\pi d^2R_p}{4}\tan\beta\sin\Omega_i, \tag{2.3}$$

$$Q_{pi}=C_{d1}A_{di}\sqrt{\frac{2|P_{pi}-P_s|}{\rho}}\operatorname{sign}(P_{pi}-P_s), \tag{2.4}$$

$$Q_{lpi}=\frac{\pi dh_{gi}^3}{12\mu(L_0+S_{pi})}(P_{pi}-P_c), \tag{2.5}$$

herein, d is piston diameter, h_{gi} is the piston-cylinder radial clearance of the i–th piston, L_0 is the initial length of the leakage path in the piston, P_c is the pressure of the case drain chamber, and C_{d1} is flow discharge coefficient. Symbols μ and ρ represent the absolute viscosity and the density of the fluid, respectively. The discharge area A_{di} of the i-th piston port, which establishes a flow path to the discharge chamber within the valve plate, is provided in Ref. [9]:

$$A_{di}=\begin{cases}\dfrac{(\Omega_i+13)^2\pi R_p}{360\times22}(R_1-R_2), & -13^\circ<\Omega_i<9^\circ\\ \dfrac{(\Omega_i-9)\pi}{360}(R_1^2-R_2^2)+\dfrac{22\pi R_p}{360}(R_1-R_2), & 9^\circ<\Omega_i<17^\circ\\ \dfrac{(\Omega_i-9)\pi}{360}(R_1^2-R_2^2)+\left[\dfrac{22^2-(\Omega_i-13)^2}{360\times22}\right]\pi R_p(R_1-R_2), & 17^\circ<\Omega_i<39^\circ\\ \dfrac{30\pi}{360}(R_1^2-R_2^2), & 39^\circ<\Omega_i<141^\circ\\ \dfrac{30(\Omega_i-141)\pi}{360}(R_1^2-R_2^2), & 141^\circ<\Omega_i<171^\circ\\ 0, & 171^\circ<\Omega_i<347^\circ\end{cases} \tag{2.6}$$

where R_1 and R_2 are outer and inner radius of the discharge kidney port in the valve plate, respectively. For a more detailed explanation of the expressions related to the discharge area, refer to Ref. [15].

The pump outlet pressure P_s can be calculated from the total discharge flow Q_p and the outlet flow Q_s by:

$$\dot{P}_s=\frac{B}{V_c}(Q_p-Q_s), \tag{2.7}$$

with

$$Q_p=\sum_1^m Q_{pi}, \tag{2.8}$$

end

$$Q_s = C_{d2} A_v \sqrt{\frac{2P_s}{\rho}}, \tag{2.9}$$

where V_c denotes the discharge chamber control volume, C_{d2} is the flow discharge coefficients, and A_v denotes the area of the throttle valve.

By integrating Eq. (2.1) and Eq. (2.7), we derive a system of (m+1) first-order differential equations that govern m piston pressure variables and the pump outlet pressure.

3. Mathematical framework

The numerical method for solving the system of differential equations governing the pump dynamic behavior will be presented. Additionally, the KL - based surrogate modeling technique will be introduced to represent pump responses over time using a finite set of reduced variables.

3.1. Runge-Kutta scheme

As previously discussed, the mathematical model of the pump operation is formulated by a system of ordinary differential equations, which collectively describe the evolution of pressure variables within the system:

$$\frac{d\boldsymbol{P}}{dt} = \Gamma(\boldsymbol{P}, t), \text{ with } \boldsymbol{P} = \left[\left\{P_{pi}\right\}_{m\times 1} \quad P_s\right] \tag{3.1}$$

This section recalls the forth-order RK scheme employed to solve the differential equation system shown in Eq. (3.1) over the interval $t \in [t_0, t_f]$ and the initial function $\boldsymbol{P}(t_0) = \boldsymbol{P}_0$. The computational time is divided into N subintervals with a step size $h = t_f/N$. At each time step $t_{n+1} = t_0 + nh$, the function value $\boldsymbol{P}(t_{n+1})$ is iteratively updated from its previous state $\boldsymbol{P}(t_n)$ at $t_n = t_0 + (n-1)h$ as:

$$\boldsymbol{P}_{n+1} = \boldsymbol{P}_n + \frac{h}{6}(\boldsymbol{k}_1 + 2\boldsymbol{k}_2 + 2\boldsymbol{k}_3 + \boldsymbol{k}_4), \tag{3.2}$$

where the intermediate coefficient vectors expressed as:

$$\begin{aligned}
\boldsymbol{k}_1 &= \Gamma(t, \boldsymbol{P}),\\
\boldsymbol{k}_2 &= \Gamma\left(t + \frac{h}{2}, \boldsymbol{P} + \frac{\boldsymbol{k}_1}{2}h\right),\\
\boldsymbol{k}_3 &= \Gamma\left(t + \frac{h}{2}, \boldsymbol{P} + \frac{\boldsymbol{k}_2}{2}h\right),\\
\boldsymbol{k}_4 &= \Gamma(t + h, \boldsymbol{P} + \boldsymbol{k}_3 h).
\end{aligned} \tag{3.3}$$

A comprehensive convergence analysis is conducted for the numerical simulation of the pump dynamic characteristics, with a particular emphasis on the outlet pressure. Initially, the relationship between the pressure difference, denoted as dP_s, and the grid number difference, denoted as dN, at the grid levels (i + 1) and (i) is established.

$$\frac{dP_s}{dN}\left(= \frac{P_s^{(i+1)} - P_s^{(i)}}{N^{(i+1)} - N^{(i)}}\right) = f(N). \tag{3.4}$$

Assuming that the above function $f(N)$ is integrable, the relative error of the numerical computation at grid level N can be approximated:

$$\dot{o}_N\left(= \frac{P_s^{(N_\infty)} - P_s^{(N)}}{P_s^{(N)}}\right) = \frac{1}{P_s^{(N)}}\int_N^{N_\infty} f(N)dN. \tag{3.5}$$

3.2. Karhunen– Loève decomposition

This section aims to construct a surrogate model that captures the relationship between key system parameters—encompassing both geometric and operational factors—and the dynamic response over the characterization period $t \in T$. Let $\boldsymbol{x} \in R^D$ represents the input parameter vector within a D-dimensional investigation space, and assume that $\boldsymbol{x} \mapsto J(t;\boldsymbol{x})$ denotes the forward mapping of interest. For brevity, the response function $J(t;\boldsymbol{x})$ will be denoted as $J(t)$ in the subsequent analysis. This response function can be systematically decomposed using the KL expansion [22, 23], facilitating an efficient representation of its stochastic variations.

$$J(t) = \underline{J}(t) + \sum_{i=1}^{\infty}\sqrt{\lambda_i}\eta_i\varphi_i(t), \tag{3.6}$$

herein, $t \mapsto J(t)$ represents the mean function of the dynamic response, defined as $\underline{J}(t) = E\{J(t)\}$ for all $t \in T$. The set of pairs $\{\lambda_i,\varphi_i\}_{i\geq 1}$ corresponds to the eigenvalues and eigenfunctions of the covariance operator $C(t,t')$ satisfying the following integral equation:

$$\int_T C(t,t')\varphi_i(t')dt' = \lambda_i\varphi_i(t), \tag{3.7}$$

and the reduced variables $\{\eta_i\}_{i\geq 1}$ are centered, mutually uncorrelated, and have unit variance. They are estimated by,

$$\eta_i = \frac{1}{\sqrt{\lambda_i}}\langle J(t) - \underline{J}(t), \varphi_i(t)\rangle. \tag{3.8}$$

The operator $\langle .,. \rangle$ represents the inner product, which is defined as:

$$\langle f, g\rangle = \int_T f(t)g(t)dt. \tag{3.9}$$

The series representation in Eq. (3.6), truncated at order p, is written as:

$$J(t) = \underline{J}(t) + \sum_{i=1}^{p} \sqrt{\lambda_i}\eta_i\varphi_i(t), \qquad (3.10)$$

where p can be determined based on a convergence analysis (i.e., $\lim_{p\to\infty} J_p = J$).

To quantify the convergence characteristics of the truncated KL expansion, the following two functions are utilized. First, the required number of realizations to achieve convergence is assessed by evaluating the function Cov(N_s), defined as:

$$\mathrm{Cov}(N_s) = \left\| \left[\tilde{C}(N_s)\right] \right\|, \qquad (3.11)$$

where $\left[\tilde{C}\right]$ represents the covariance matrix of the discretized process.

To identify the truncation order p for the statistical estimator, the second convergence property is analysed by the error function Err(p) defined as,

$$\mathrm{Err}(p) = 1 - \frac{\sum_{i=1}^{p}\lambda_i}{\mathrm{tr}\left(\left[\tilde{C}\right]\right)}. \qquad (3.12)$$

4. Results

Within a given piston pump configuration, the method developed in this study will be applied to evaluate the convergence characteristics and the potential effectiveness in investigating the dynamics of the pump system while accounting for the uncertainty of model parameters.

4.1. Case study and convergence assessment

As an illustrated case study, an axial piston pump configuration is chosen with the following parameters [9, 21]: A_p = 8.343E-05 m^2, A_v = 4.457E-06 m^2, B = 8.547E+08 Pa, C_{d1} = 0.675, C_{d2} = 0.610, d = 1.031E-02 m, h_g = 45 µm, L_0 = 0.0145 m, P_c = 1E+05 Pa, R = 5.162E-03 m, R_1 = 0.0238 m, R_2 = 0.0204 m, R_p =0.0221 m, m = 9, V_0 = 1.543E-06 m^3, V_c = 3.156E-05 m^3, V_d = 2.0540E- 07 m^3, α = 0.698 , β = 0.335, ω = 188.4 1/s, μ =5.855E-02 Ns/m^2, ρ = 860 kg/m^3. In this work, initial pressures are given as $P_{pi}(t_0)$ = 1E+07 Pa and $P_s(t_0)$ = 9E+06 Pa. All computations were performed on a computer with an Intel(R) Core(TM) i7-4500U CPU @ 1.80 GHz (boost up to 2.40GHz) and 8.00 GB of RAM. For t_f = 0.05 s with a step of 1 µs, the computation time is approximately 58 seconds.

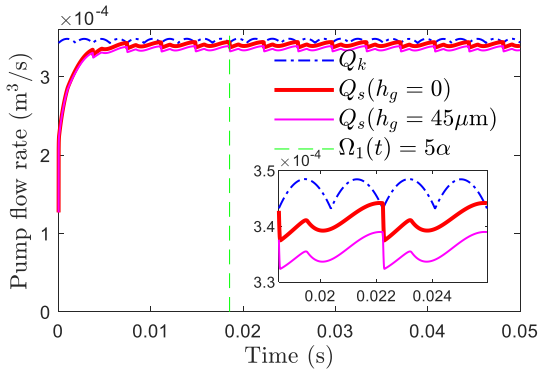

Figure 2: Graphs of the calculated flow rate responses: outlet flow (solid lines, thick and thin curves are for h_{gi} = 0 and h_{gi} = 45 µm, respectively) and theoretical flow (dashed-dot line).

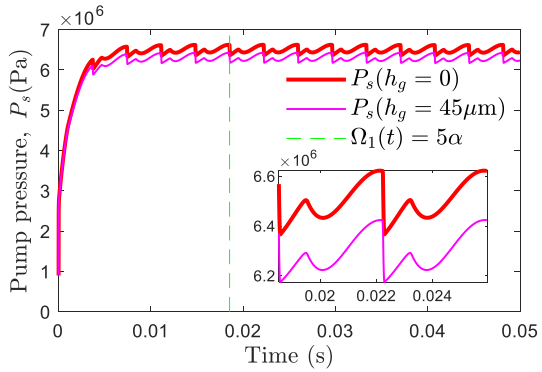

Figure 3: Results of the calculated outlet pressure response for the case of with (thick line) and without (thin line) the radical clearance.

As shown in Figs. 2-3, two calculated pump characteristics are provided including the outlet flow rate (Fig. 2) and the outlet pump pressure (Fig. 3). The pump flow rate and pressure results indicate that the pump starts to reach its working value when the first piston completes its cycle (when $\Omega_1(t) = 5\alpha$ or at the time $t = 5\alpha/\omega \sim 0.0185$ s) of pumping oil into the plate valve. The highest ripple occurs at the moment when the pumping system completes one delay phase angle α (i.e., angular distance between two consecutive pistons). These observed results are consistent with previously published works [9,13]. An interesting feature appears on the pump characteristic curve, where the temporal evolution of the characteristics differs entirely from the theoretical predictions (see the enlarged views extracted in Figs. 2-3). This finding is consistent with the impact of the valve plate geometry on the pump response, provided in Ref. [33]. The calculated results show that the outlet pressure and flow rate exhibit a cyclic variation of $T_\alpha = \alpha/\omega \sim 0.0037$ s. It can be seen that the actual f low rate (maximum

value of 3.4422E-04 m^3/s and 3.3902E-04 m^3/s for cases of h_g = 0 and h_g = 45 μm, respectively) of the pump is smaller than the theoretical flow rate (maximum value of 3.4851E-04 m^3/s). The ripple level of the flow characteristic curve is quite similar, with 1.97% for the actual pump flow curve compared to 1.54% for the theoretical flow one. The pressure characteristics exhibit a higher ripple level of approximately 4% for both cases: the pump with and without the wear gap h_g between the piston and the cylinder block. Since other characteristics are mathematically related to the pump's pressure response (see Eq. (2.9) as an example), the remaining discussions will mainly focus on the working pressure characteristics of the pump.

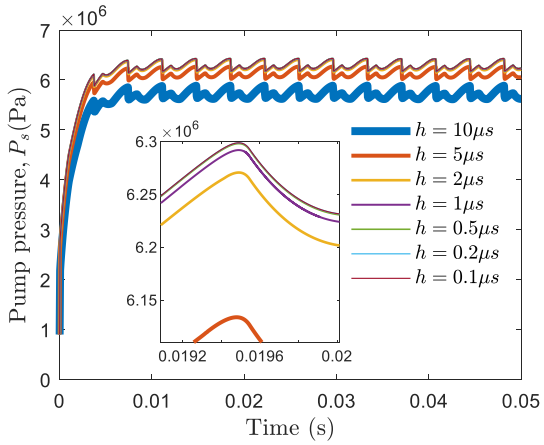

Figure 4: Results of the computed outlet pump pressure with different time steps *h* from 0.1 μs to 10 μs.

To examine the convergence characteristics of the RK scheme, seven values of the investigated computation step include *h* = {10 5 2 1 0.5 0.2 0.1} μs corresponding to a set of grid levels given as $N = t_f/h$. It can be noted that with a time step of 0.1 μs, the computation time becomes a challenge (i.e., taking more than an hour and a half).

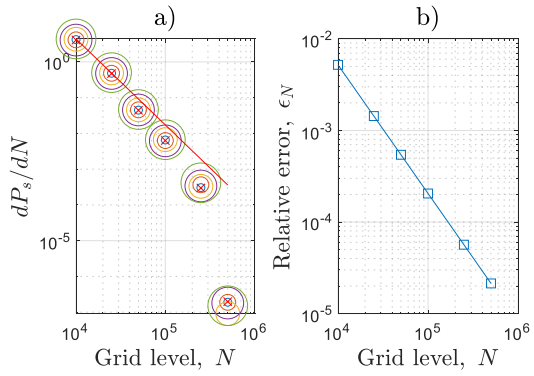

Figure 5: Results of (a) convergence analysis in pressure calculations (at several calculation times and the average pressure shown in circle and cross markers, respectively) and (b) the corresponding relative error $N \mapsto \varepsilon_N$.

Figure 4 shows the working pressure results of the pump at different calculated values of the grid level. It is found that, when decreasing the value of the calculation time step, the pressure value above the survey time gradually increases and converges. For details, Figure 5 presents the convergence level of the calculation results to be quantified through the pressure value at five calculation times (circle markers) corresponding to *t* = {0.02 0.025 0.035 0.04 0.05} s and the average pressure value (cross markers). To evaluate the convergence characteristics of the calculation results, we obtain the fitting function for all considered cases, $f(N) = \exp(a)N^b$ with a = 23.63 and b = -2.405. The error ϵ_N in Eq. (3.5) at the grid level of $N_{\max}$ can be approximated as,

$$\epsilon_N = \frac{\exp(a)}{P_s^{(N_{\max})}} \frac{N_\infty^{b+1} - N_{\max}^{b+1}}{(b+1)}. \tag{4.1}$$

Taking $N_\infty \to \infty$ and $b < -1$, the above expression simplifies to:

$$\epsilon_N = -\frac{\exp(a)}{P_s^{(N_{\max})}} \frac{N_{\max}^{b+1}}{(b+1)}. \tag{4.2}$$

Using Eq. (4.2) we can estimate the relative error for a given grid level. For all testing cases, the tolerance error $\epsilon_N < 1\times10^{-3}$ can be reached with a grid level $N = 5\times10^5$ (or a time step of *h* = 1 μs) as shown in Fig. 5b.

4.2. Statistical reduction of computational surrogates

This section examines the convergence analysis of reduced-order models for pump performance with considering the uncertainties in the system parameters as $R^D \ni \boldsymbol{x} = [A_p\ A_v\ B\ \beta\ d\ L_0\ r_0\ R\ R_1\ R_2\ R\ \mu\ V_0\ V_c\ V_d]$ with D = 15. Assume that the system parameters of the pump dynamic computational model have the same distribution function. Herein, two types of distributions for the system parameters are considered, normal distribution and uniform distribution corresponding to their tested samples, denoted by $\mathrm{NorS} := \boldsymbol{x}_N \in N(\bar{x}, \sigma_x)$ and $\mathrm{UniS} := \boldsymbol{x}_U \in U(\bar{x} - \xi_x, \bar{x} + \xi_x)$, respectively. It can be noted that the mean value $\bar{x}$ is taken from the deterministic values presented in Section 4.1. To initialize the survey data, the pump configuration parameters are built as follows. To consider the degree of uncertainty of the pressure response of the pump, the system parameters are assumed to be the same uncertainty level as $\sigma_x = \sigma_N \bar{x}$ and $\xi_x = \xi_U \bar{x}$. In the later

calculations, these values σ_N = 0.01 and ξ_U = 0.015 are selected. Due to the periodic response characteristics, the value t_f is chosen to correspond to the time required for the pump to rotate by 10α, corresponding to t_f = 0.0371 s. The influence of uncertainty factors on pump pressure characteristics will be considered simultaneously with the performance comparison

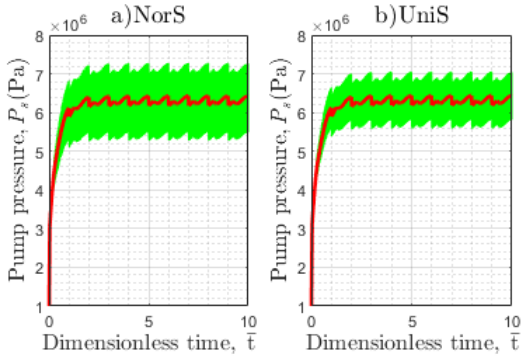

Figure 6: Effects of uncertainties in model parameters on the pump pressure for the (a) NorS and UniS (b) scenarios. The colour bound and the centre curve show the variation of the average outlet pump pressure, respectively. Here, the sample size is taken as N_s =1000.

of the surrogate functions compared to the reference functions, from the generated data from two investigation scenarios as presented in Fig. 6. The observed results demonstrate that the pressure characteristics in the NorS scenario (i.e., left panel) have a larger standard deviation compared to the UniS scenario (i.e., right panel).

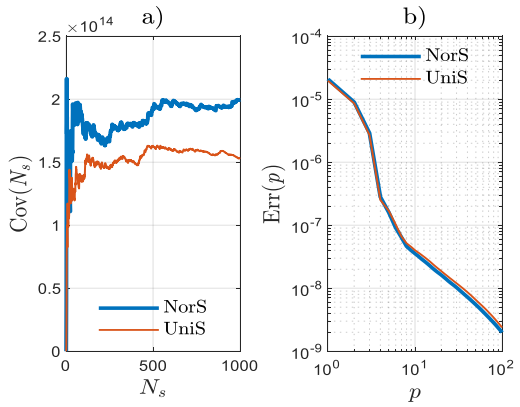

Figure 7: Convergence property of the truncated KL expansions: a) $N_s \mapsto \left\| \left[\tilde{C}(N_s) \right] \right\|$ and b) $p \mapsto \mathrm{Err}(p)$.

The interval is chosen to ensure that that the first piston completes five phase delay angles to reach a steady state value (see Fig. 2). For simplicity of presentation, dimensionless time is used as $\bar{t} := (\Omega_1(t) - \Omega_s)/\alpha$. It is clear that, by choosing $\Omega_s = 5\alpha$, the dimensionless time t varies from 0 to 5.

The convergence properties of the KL truncated expansions are shown in Fig. 7 (left panel: functions $N_s \mapsto \left\| \left[\tilde{C}(N_s) \right] \right\|$, right part: maps $p \mapsto \mathrm{Err}(p)$). In general, the convergence characteristics of the two samples exhibit a high degree of similarity. Reasonable convergence is observed for N_s = 1000, which is therefore adopted for the subsequent calculations. Moreover, the error remains below 1x10^{-4}, 1x10^{-6}, and 1x10^{-8} for p = 1, p = 4, and p = 22, respectively. In the following, a truncation order of p = 10 is considered.

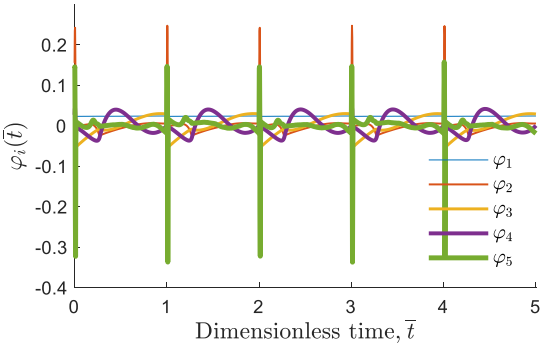

Figure 8: Plots of the five first eigenfunctions.

$t \mapsto \varphi_i(t)$ which are used to represent the outlet pump pressure estimated from the numerical calculations.

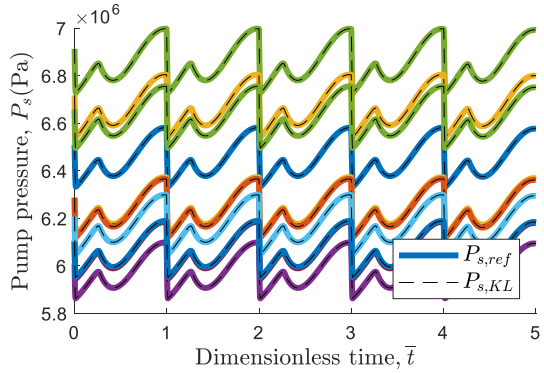

Figure 9: Graphs of the ten reference functions $\bar{t} \mapsto P_{s,ref}(\bar{t})$ (continuous lines) and the corresponding surrogates $\bar{t} \mapsto P_{s,KL}(\bar{t})$ with p = 10 (dashed lines).

As displayed in Fig. 8, the results of the five first eigenfunctions $\{\bar{t} \mapsto \varphi_i(\bar{t})\}_{i=1}^{5}$ indicate that all these functions exhibit a non-smooth region around the time when the individual pump piston moves through the transition zone in the valve plate [14]. Using the calcualted truncation order, recuduced variables, and eigenfunctions mentioned above, a quantitative comparison between the reference functions $P_{s,ref}$ and the surrogate functions $P_{s,KL}$ is illustrated in Fig. 9, for a set of ten selected pump configurations from the NorS sample data.

Figure 10 presents the pressure distribution functions at five different calculation points, comparing the selected reference pressure (solid lines), the corresponding surrogate pressures (dashed lines), and the fitting normal distributions (dotted lines). The results demonstrate the good predictive performance of the surrogate model, while also reflecting the similarity of the pump's characteristics to a normal distribution, as shown by the fitting curves.

Finally, we assess the four statistical measures that describe the shape of the pump pressure distributions, including [24]: mean value μ_{Ps}, standard deviation σ_{Ps}, Kurtosis coefficient K_u and Skewness coefficient S_k for both scenarios considered.

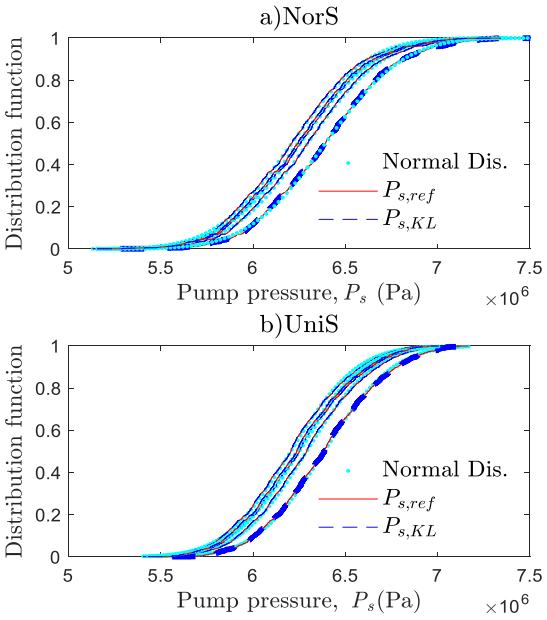

Figure 10: Graphs of the five distribution functions of the selected reference pressure $P_{s,ref}$ (continuous lines), surrogate pressures $P_{s,KL}$ (dashed lines),and the fitting normal distributions (dots).

The results presented in Fig. 11 illustrate that the uncertainty level or the standard deviation of the pump pressure with the NorS scenario is larger than that with the UniS scenario, corresponding to values of 3.25E+5 Pa and 2.85E+5 Pa (calculated through the average values plotted in Figs. 11a-b). The uncertainty in the pump pressure response (that is, $[\sigma_{Ps}/\mu_{Ps}]_{\text{NorS}} \sim 0.052$ and $[\sigma_{Ps}/\mu_{Ps}]_{\text{UniS}} \sim 0.045$) has a significantly higher value than that of the system parameters (i.e., $\sigma_N = 0.01$, $\xi_U = 0.015$). From the measure characteristics shown in Figs. 11-12, it is again possible to confirm that the numerical evaluations of the pump pressure distribution characteristics determined from the reference data and the surrogate data have a very high similarity.

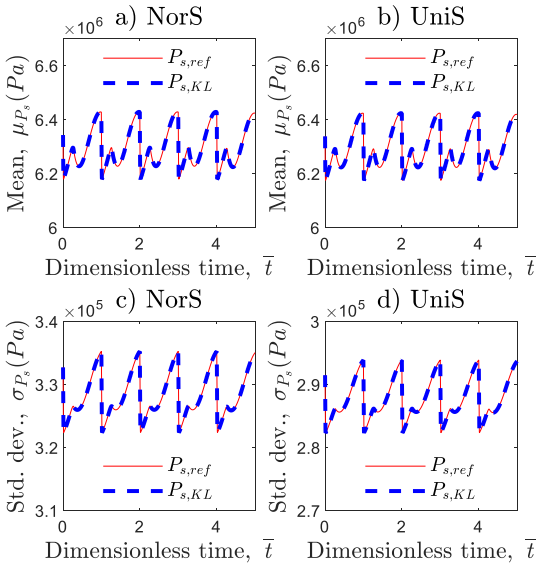

Figure 11: Results of the mean (a,b) and standard deviation (c,d) characteristics of the pressure distribution functions for the UniS and NorS samples obtained from the calculated reference function (continuous line) and the reconstructed surrogate response (dashed line).

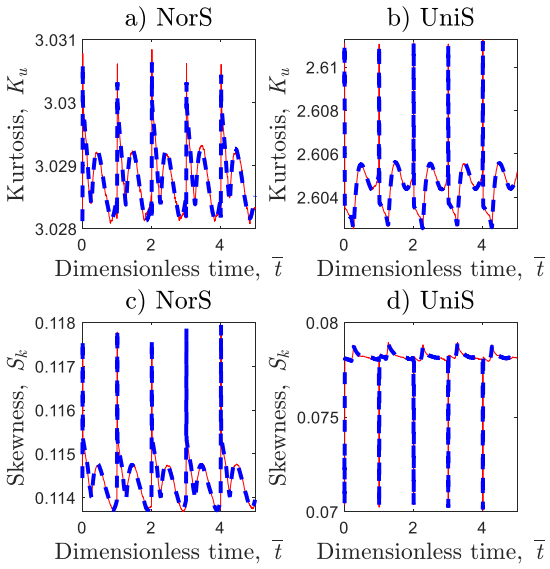

Figure 12: Results of the Kurtosis (a,b) and Skewness (c,d) measures of the outlet pressure distribution functions, legends as shown in Fig 11.

5. Discussion

In this paper, the dynamic characteristics under uncertainties of axial piston pumps are studied using numerical methods based on the RK scheme and KL expansion. From the observed results, it can be stated that the dynamic model of axial piston pumps can be solved using the forth-order RK method, which ensures stable convergence over the entire investigated time

period. The reconstructed surrogate model, based on KL expansion with a low truncation order, can successfully predict the dynamic responses of axial piston pumps, even in the presence of non-smooth regions caused by transition periods during operation. The pump response appears to exhibit a higher degree of uncertainty than the uncertainty in the system configuration parameters. When the system parameters follow either a uniform or normal distribution, the system response follows a normal distribution function. A possible extension of the research presented in this paper is to consider the uncertainty characteristics of each parameter and evaluate their sensitivity. In this context, advanced computational methods can be employed to reduce the sample size or maintain the large sample size by generated data based on the limited reference sample.

Acknowledgments

This work is supported by Le Quy Don Technical University (Grant No. 24.1.64).

References

[1] N.D. Manring, R.C. Fales, Hydraulic control systems, John Wiley & Sons, 2019.

[2] P. Dransfield, Hydraulic control systems—design and analysis of their dynamics, Lecture Notes in Control and Information Sciences; Springer: Berlin/Heidelberg, Germany, **33**, 1981.

[3] J.M. Bergada, S. Kumar, J. Watton, Axial piston pumps, new trends and development, in book: Fluid Dynamics, Mechanical Applications and Role in Engineering, Nova Science Publishers, New York, 2012.

[4] S. Guo, J. Chen, Y. Lu, Y. Wang, H. Dong, Hydraulic piston pump in civil aircraft: Current status, future directions and critical technologies, Chinese Journal of Aeronautics, **33**, 1, 16-30, 2020.

[5] P. Ying, H.Tang, L. Chen, Y. Ren, A. Kumar, Dynamic modeling and vibration characteristics of multibody system in axial piston pump, Alexandria Engineering Journal, **62**, 523-540, 2023.

[6] Y. Yang, L. Ding, J. Xiao, G. Fang, J. Li, Current status and applications for hydraulic pump fault diagnosis: A review, Sensors, **22**, 24, 9714, 2022.

[7] P.D. Srivyas, S. Singh, B. Singh, Study of various maintenance approaches types of failure and failure detection techniques used in hydraulic pumps: A review, Industrial Engineering Journal, **5**, 27-35, 2017.

[8] H.A. Babikir, M. Abd Elaziz, A.H. Elsheikh, E.A. Showaib, M. Elhadary, D. Wu, Y. Liu, Noise prediction of axial piston pump based on different valve materials using a modified artificial neural network model, Alexandria Engineering Journal, **58**, 3, 1077-1087, 2019.

[9] Z.E. Li, Condition monitoring of axial piston pump, Dissertation, Saskatoon: University of Saskatchewan; 2005.

[10] G.P. Kavanagh, The dynamic modelling of an axial piston hydraulic pump, University of Saskatchewan, 1987.

[11] W. Latas, J. Stojek, Dynamic model of axial piston swash-plate pump for diagnostics of wear in elements, Archive of Mechanical Engineering, **58**, 2, 135-155, 2011.

[12] S. Ye, J. Zhang, B. Xu, L. Hou, J. Xiang, H. Tang, A theoretical dynamic model to study the vibration response characteristics of an axial piston pump, Mechanical Systems and Signal Processing, 150, 107237, 2021.

[13] B. Zhang, J. Ma, H. Hong, H. Yang, Y. Fang, Analysis of the flow dynamics characteristics of an axial piston pump based on the computational fluid dynamics method, Engineering Applications of Computational Fluid Mechanics, **11**, 1, 86-95, 2017.

[14] B. Xu, Y.H. Sun, J.H. Zhang, T. Sun, Z.B. Mao, A new design method for the transition region of the valve plate for an axial piston pump, Journal of Zhejiang University-SCIENCE A, **3**, 16, 229-240, 2015.

[15] I.S. Cho, J. Jung, A study on the pressure ripple characteristics in a bent-axis type oil hydraulic piston pump, Journal of Mechanical Science and Technology, **27**, 3713-3719, 2013.

[16] T.R. Milind, M. Mitra, A study on the dynamics and vibration behavior of an axial piston pump using combined MBD/FE approach, Procedia Engineering, **144**, 452-460, 2016.

[17] K.A. Harrison, K.A. Edge, Reduction of axial piston pump pressure ripple, Proceedings of the Institution of Mechanical Engineers, Part I: Journal of Systems and Control Engineering, **214**, 1, 53-64, 2000.

[18] G. Paulmann, G. Mkadara, Condition Monitoring of hydraulic pumps-lessons learnt, Universitätsbibliothek der RWTH Aachen, 2018.

[19] N. Helwig, E. Pignanelli, A. Schütze, Condition monitoring of a complex hydraulic system using

multivariate statistics, in 2015 IEEE International Instrumentation and Measurement Technology Conference (I2MTC) Proceedings, IEEE, 2015.

[20] C.S. Byington, M. Watson, D. Edwards, B. Dunkin, In-line health monitoring system for hydraulic pumps and motors, in 2003 IEEE Aerospace Conference Proceedings (Cat. No. 03TH8652), IEEE, 2003.

[21] N. Kumar, R. Kumar, B.K. Sarkar, S. Maity, Condition monitoring of hydraulic transmission system with variable displacement axial piston pump and fixed displacement motor, Materials Today: Proceedings, **46**, 9758-9765, 2021.

[22] H.L. Van Trees, Detection, estimation, and modulation theory, part I: Detection, estimation, and linear modulation theory John Wiley & Sons, 2004.

[23] G.J. Lord, C.E. Powell, T. Shardlow, An introduction to computational stochastic PDEs, **50**, Cambridge University Press, 2014.

[24] W.H. Press, Numerical recipes 3rd edition: The art of scientific computing, Cambridge university press, 2007.

[25] D.L. Rivera, M.R. Scholz, M. Fritscher, M. Krauss, K. Schilling, Towards a predictive maintenance system of a hydraulic pump, IFAC-PapersOnLine, **51**, 11, 447-452, 2018.

[26] L. Wang, H. Yin, W. Sun, Fault diagnosis and predictive maintenance for hydraulic system based on digital twin model, AIP Advances, **12**, 6, 2022.

[27] F. Wu, J. Tang, Z. Jiang, Y. Sun, Z. Chen, B. Guo, The remaining useful life prediction method of a hydraulic pump under unknown degradation model with limited data, Sensors, **23**, 13, 5931, 2023.

[28] M.H. Nguyen, K.K. Ahn, Output feedback robust tracking control for a variable-speed pump-controlled hydraulic system subject to mismatched uncertainties, Mathematics, **11**, 8, 1783, 2023. 15

[29] N.D. Manring, Measuring pump efficiency: Uncertainty considerations, ASME Journal of Energy Resources Technology, **127**, 280–284, 2005.

[30] H.D. Feng, L. Xu, R.P. Xu, L.J. Wu, X.H. Shi, J.D. Yan, T.Y. Wang, Uncertainty analysis using the thermodynamic method of pump efficiency testing, Proceedings of the Institution of Mechanical Engineers, Part C: Journal of Mechanical Engineering Science, **218**, 5, 543-555, 2004.

[31] S. Salehi, M. Raisee, M.J. Cervantes, A. Nourbakhsh, On the flow field and performance of a centrifugal pump under operational and geometrical uncertainties, Applied Mathematical Modelling, **61**, 540-560, 2018.

[32] T. Kato, S. Sakai, R. Arai, On the uncertainty analysis via low frequency inputs for hydraulic cylinder dynamics, JFPS International Journal of Fluid Power System, **15**, 3, 95-100, 2022.

[33] D. Wang, C. Chen, H. Dong, Investigation of the pressure fluctuation of piston chambers with variable slot geometry, Machines, **11**, 2, 225, 2023.